

An Investigation on the Anti-Corrosion Characteristics of Stainless Steel Cladding

Anup Kumar Verma¹, Bidhan Chandra Biswas², Protap Roy³, Samiran De⁴, Sukanta Saren⁵ and Santanu Das⁶
Department of Mechanical Engineering, Kalyani Government Engineering College, Kalyani- 741235, West Bengal.
Email: ¹anupkgec@rediffmail.com, ²bidhan0202@gmail.com, ³protap.7002@yahoo.in, ⁴samirdandulia@gmail.com,
⁵skntsrn@gmail.com, ⁶sdas.me@gmail.com



DOI : 10.22486/iwj/2017/v50/i3/158282

ABSTRACT

Cladding through GMAW can be done on surfaces of components and structures exposed to corrosive environment to raise their service life. Corrosion resistant materials are clad up on to a corrosion prone material up to a desired thickness. Since clad materials are basically of different compositions, they are dissimilar in nature. In the present work, cladding of austenitic stainless steel (316) is done on to low alloy steel specimens under varying parametric combinations. Clad quality including metallography is studied on clad specimens at different locations of it. Corrosion tests performed on clad specimens show substantially less corrosion pits present on the surface of clad portions than that on the surface of unclad portion. At a weld voltage of 26 V, weld current of 145 A, and weld speed of 535.8 mm/min, with a heat input of 0.338 kJ/mm, corrosion rate is observed to be the minimum among the experiments conducted, and hence, can be recommended to adopt.

Key words: Cladding; austenitic stainless steel; corrosion; welding, GMAW; heat input.

1.0 INTRODUCTION

Cladding on cheap, corrosion prone metallic components and structures with a corrosion resistant material ensures their durability. Therefore, it lowers frequency of replacement, and overall maintenance cost [1]. Among different processes of cladding, gas metal arc welding is often employed for cladding ferrous materials effectively [2].

Composition of clad material, quality of bond, and weld bead geometry can be considered to determine strength and quality of cladding, and selection of appropriate process parameters can render good weld bead and clad quality. Many investigations have been made in the past in this direction [3-8]. Under varying process parameters, research works have been carried out on different workpiece materials using different electrode materials. Few investigations have been done to evaluate the appropriate process parameters by employing some optimizing algorithms, such as the Analytical

Hierarchy Process (AHP) [6], Simulated Annealing (SA) [7], Grey Relational Analysis [8], Neural Networks (NN), etc. Different kinds of stainless steels [9, 10], particularly, duplex stainless steels [11-13] and austenitic stainless steels [14-18] have been tried for cladding to have high resistance against corrosion. Different corrosion tests have been explored [18] to evaluate anti-corrosive nature of cladding. Gas metal arc welding (GMAW) has been observed [11, 16] to show good quality cladding under a typical combination of process parameters using austenitic as well as duplex stainless steel electrodes. Optimization of weld bead geometry has also been explored by some other researchers [19] using detailed experiments and also by doing post data analysis using some algorithms. In fine, many investigations have been taken up in the past for evaluating suitable process parameters in welding to suite its applicability.

The present investigation aims at observing the characteristics of austenitic stainless steel cladding using gas metal arc

welding (GMAW) with 100% CO₂ as shield. The experimental work is carried out with 316 stainless steel wire of 1.2 mm diameter on low alloy steel specimens to find out an optimum set of process conditions within the domain of present experiments.

2.0 DETAILS OF EXPERIMENTAL WORK

For the present investigation, a GMAW machine (model: AutoK 400 of ESAB, India) is employed. Cladding is done using GMAW by applying 100% CO₂ gas shield. Linear motion of welding torch along a guided path is provided using a motor driven attachment. CO₂ gas is supplied at a flow rate of 18 litre/min. Low alloy steel specimens have the size of 100 mm x 50 mm x 6 mm. Passes are done at an overlap of 50%. Austenitic stainless steel (grade 316) wire of 1.2 mm diameter is used in this experimental investigation. Composition of austenitic stainless steel wire used and base material are shown in **Table 1** and **Table 2** respectively. The base material has carbon of 0.157% with 0.227% silicon, 0.549% manganese and trace amount of other elements. For this composition, the base plate has good weldability, formability and machinability; however, it corrodes fast under adverse environment. On the other hand, 316 austenitic stainless steel electrode has 0.084% carbon, 0.257% silicon, 0.937% manganese, 17.322% chromium, 8.192% nickel, 0.304% molybdenum and 0.197% cobalt. This composition of steel is expected to make strong, heat resistant and corrosion resistant weld.

Weld voltage and weld current chosen are 26V and 28V, and 130 A and 145A respectively. Weld speed is varied within 414.6 to 536.4 mm/min. Corresponding heat input varies in the range of 0.338 to 0.412 kJ/mm. Different experimental runs and corresponding heat inputs are shown in **Table 3**. Heat input is calculated by using Equation (1) [17, 18].

$$Q = (60 V I \eta) / (1000 S) \tag{1}$$

where,

Q = heat input (kJ/mm)

V = weld voltage (V)

I = weld current (A)

S = welding speed (mm/min)

η = process efficiency; for GMAW it is taken as 0.8.

Hardness of the specimen at different locations is measured before and after cladding using a Lab Equipment & Chemicals, Kolkata made Rockwell Hardness Tester. A carbide steel ball of 1.5875 mm diameter is employed using a load of 100 kg for this test in B scale.

Table 3 : Heat input used for weld cladding

Sl. No.	Voltage (V)	Current (A)	Welding Speed (mm/min)	Heat Input, Q (kJ/mm)
1	26	145	535.8	0.338
2	26	130	471.6	0.344
3	28	145	536.4	0.363
4	28	145	516	0.378
5	26	130	414	0.392
6	28	145	472.8	0.412

Table 1 : Composition of base plate

%C	%Si	%Mn	%P	%S	%Cr	%Ni	%W	%Sn	%Cu	%Ta	%Zn	%As
0.157	0.227	0.549	0.097	0.051	0.016	0.034	0.03	0.013	0.056	0.013	0.018	0.072

Table 2 : Composition of 316 austenitic stainless steel filler

%C	%Si	%Mn	%P	%S	%Cr	%W	%Mo	%Ni	%Co	%Cu	%Ti	%V	%Nb	%Ce
0.084	0.257	0.937	0.029	0.015	17.322	0.025	0.304	8.192	0.197	0.401	0.025	0.05	0.048	0.016

Bead geometry influences mechanical property of a weld [19-20]. Keeping this in mind, reinforcement and penetration are measured after cutting each specimen along its cross section. Mitutoyo, Japan make tool makers microscope is used for this.

Each clad specimen is polished and etched in Kalling's No.2 reagent (100 ml ethanol, 100 ml HCL, and 5 gm CuCl₂). Microstructure is observed under a metallurgical microscope with which digital photographs are taken at 200x magnification. Corrosion test is carried by polishing and weighing samples by a digital weighing machine (model: M K 100E, Petit Balance) with 1 µgm resolution. Corrosive solution is made with a mixture of anhydrous ferric chloride, hydrochloric acid, and distilled water. Each sample is immersed into 33 ml of this solution for 24 hours with masking non-clad portion with teflon tape. Corrosion test is stopped after 24 hours, and samples are washed under running water. Samples are then dipped in ethyl alcohol, dried and weighed again. Corrosion rate is found out from the formula given in equation (2).

$$\text{Corrosion rate} = \frac{\text{weight loss}}{[\text{area exposed} \times \text{time of exposure}]} \quad (2)$$

where,

weight loss is in gm,

area exposed is in m² and

time of exposure is in hour.

3.0 RESULTS AND DISCUSSION

Results of hardness of the base material measured well beyond the weld portion or HAZ, before and after cladding are observed to be quite similar about 85 HRB. Presence of small amount of carbon and other alloying elements may have resulted in poor hardenability, and hence this observation. From equation (1), heat input is found to increase with increase in weld voltage and weld current and decrease in of welding speed. Values of reinforcement and depth of penetration are shown in **Table 4**. With an increase in heat input, penetration and reinforcement initially show an increasing tendency, followed by a decreasing nature on the whole. Depth of penetration is found to be high (1.63 mm) at experiment Nos. 3 and 4, while reinforcement is the highest (2.73 mm) at experiment No. 5 corresponding to the heat input of 0.392 kJ/mm.

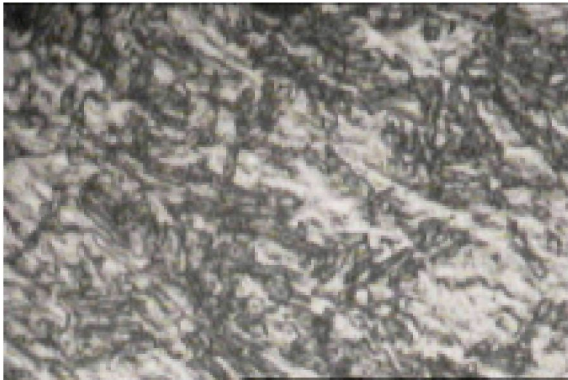
Micrographs of clad portion of specimens are shown in **Fig. 1 (a-f)**. Formation of different phases in clad portion is possible during phase transformation of austenite from the ferrite-cementite mixture. The grain growth and the final phase mostly depend on the solidification rate or cooling rate and the alloy content. Elmer et al. reported [21] that solidification modes of stainless steel alloys can be one of the five modes: single-phase austenite (A), primary austenite with second phase ferrite (AF), eutectic ferrite and eutectic austenite (E), primary ferrite with second-phase austenite (FA) and single-phase ferrite (F).

Table 4 : Bead geometry obtained from the experiment

Sl. No.	Voltage (V)	Current (A)	Welding Speed (mm/min)	Heat Input Q (kJ/mm)	Depth of penetration, P (mm)	Reinforcement R (mm)
1	26	145	535.8	0.338	1.25	1.48
2	26	130	471.6	0.344	1.38	1.48
3	28	145	536.4	0.363	1.63	1.98
4	28	145	516	0.378	1.63	2.22
5	26	130	414	0.392	1.37	2.73
6	28	145	472.8	0.412	1.51	2.08

The grain structure shown in **Fig.1(b)** indicates single phase ferrite (F) solidification with Widmanstätten austenite (γ) formation. The microstructure depicted in **Fig.1(c)** shows equiaxed fine grains of austenite (γ) in ferrite (α) matrix with precipitation of sigma (σ) phase indicating presence of α ferrite. The microstructure depicted in **Fig.1(f)** corresponding to experiment No. 6 shows epitaxial growth of single phase

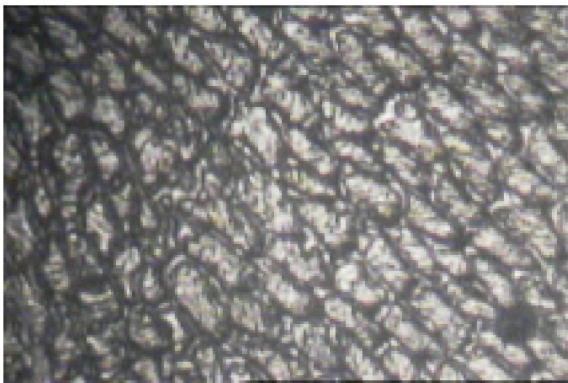
austenite (γ) grains which are darker near grain boundaries. Acicular structure of ferrite-carbide mixture [22] is seen in **Fig.1(a)**. This indicates possible precipitation of body-centered tetragonal (BCT) martensite from face-centered cubic (FCC) austenite due to high cooling rate. **Fig.1(d) & 1(e)** show single phase ferrite transformation with some transformation of austenite as Widmanstätten structure.



(a) V= 26 V, I= 145 A, S= 535.8 mm/min, Q= 0.338 kJ/mm, experiment No. 1,



(b) At V= 26 V, I= 130 A, S= 471.6mm/min, Q= 0.344 kJ/mm, experiment No. 2



(c) At V= 28 V, I= 145 A, S= 536.4mm/min, Q= 0.363 kJ/mm, experiment No. 3



(d) V= 28 V, I= 145 A, S= 516 mm/min, Q= 0.378 kJ/mm, experiment No. 4



(e) V= 26 V, I= 130 A, S= 414 mm/min, Q= 0.392 kJ/mm, experiment No. 5



(f) At V= 28 V, I= 145 A, S= 472.8 mm/min, Q= 0.412 kJ/mm, experiment No. 6

Fig.1 : Microstructure (200x) of austenitic stainless steel cladding on low alloy steel specimens

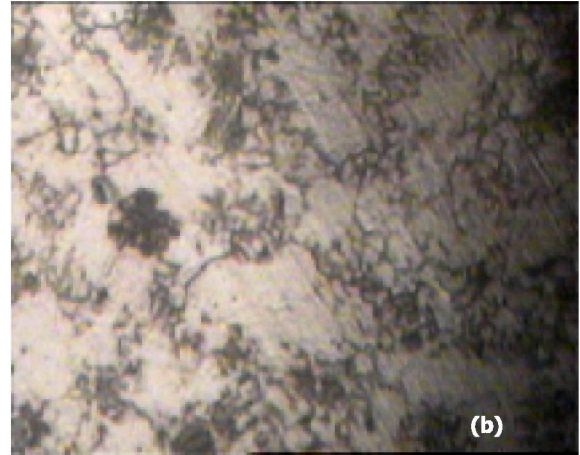
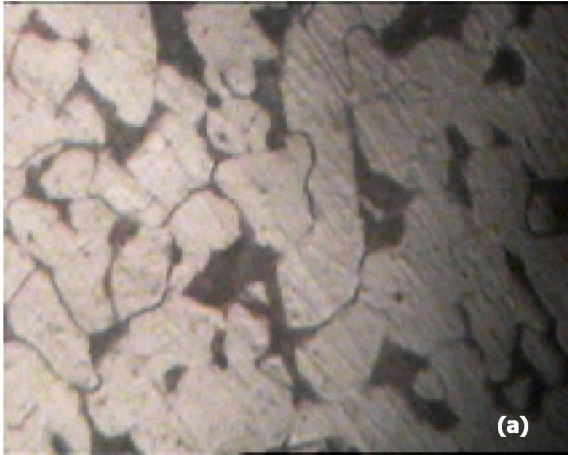


Fig.2 : View of the microstructure (200x) of the base material etched with 2% nital (a) before cladding, and (b) typically at a heat affected zone

Fig.2(a) shows the microstructure of base plate before cladding. Ferrite and pearlite with coarse grains are seen in the micrograph. In the typical microstructure of heat affected zone after cladding (**Fig.2(b)**), refinement of ferrite and pearlite grains to some extent can be observed.

Typical interface region is shown in **Fig.3(a)** and **3(b)**. **Fig.3(a)** is etched with 2% nital that causes good revelation of microstructure of low alloy steel, while Kalling's No.2 etchant gives **Fig.3(b)** showing stainless steel microstructure of clad portion. Both the figures show fairly good degree of bonding shown by penetration of clad material in to the base material.

Table 7 shows corrosion rates of clad specimens obtained under varying weld conditions. Corrosion rate is found to increase with hike in heat input up to a level. Beyond a heat

input, further increase in heat input is observed to result in lowering of corrosion rate.

It indicates substantially less corrosion rate on clad specimens expectedly. Experiment No.5 gives maximum corrosion rate than the other runs within the domain of experiments considered. Substantial improvement in corrosion resistance is observed in clad specimens under 26 V, 145 A and 535.8 mm/min weld speed condition corresponding to experimental run 1 and heat input of 0.338 kJ/min. This condition involves the lowest heat input among the present experimental conditions. At this condition, dilution may be high, and good corrosion resistance is obtained. **Fig.4(a-f)** show corrosion pits formed due to corrosion test on clad plate under different conditions.

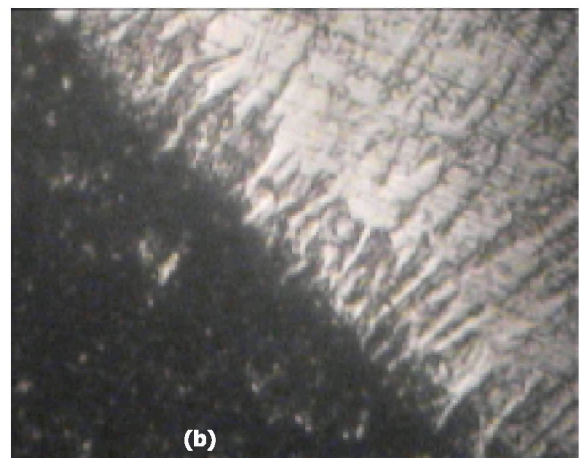


Fig.3 : View of the microstructure (200x) of the interface region of base metal and clad portion (a) etched with 2% nital, and (b) etched with Kalling's No. 2 etchant

Typical interface region is shown in **Fig.3(a)** and **3(b)**. **Fig.3(a)** is etched with 2% nital that causes good revelation of microstructure of low alloy steel, while Kalling's No.2 etchant gives **Fig.3(b)** showing stainless steel microstructure of clad portion. Both the figures show fairly good degree of bonding shown by penetration of clad material in to the base material.

Table 7 shows corrosion rates of clad specimens obtained under varying weld conditions. Corrosion rate is found to increase with hike in heat input up to a level. Beyond a heat input, further increase in heat input is observed to result in lowering of corrosion rate.

It indicates substantially less corrosion rate on clad specimens expectedly. Experiment No.5 gives maximum corrosion rate than the other runs within the domain of experiments considered. Substantial improvement in corrosion resistance is observed in clad specimens under 26 V, 145 A and 535.8 mm/min weld speed condition corresponding to experimental run 1 and heat input of 0.338 kJ/min. This condition involves the lowest heat input among the present experimental conditions. At this condition, dilution may be high, and good corrosion resistance is obtained. **Fig.4(a-f)** show corrosion pits formed due to corrosion test on clad plate under different conditions.

Fig.4(a) and **4(b)** show few large pits at some regions. But **Fig.4(c)** shows distributed large pits all through the specimen.

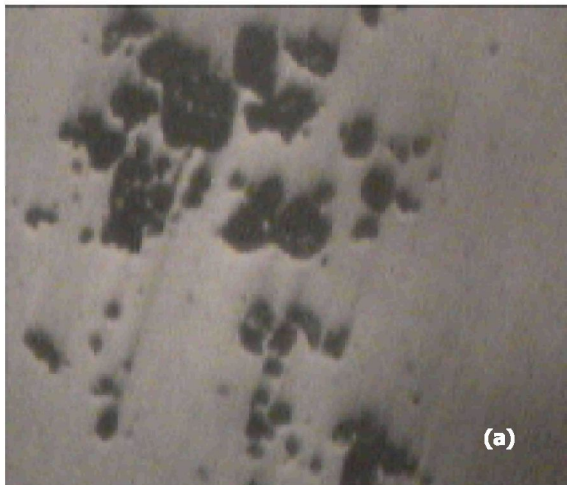
Table 6 : Corrosion rate of base plates

Sl. No.	Corrosion rate (gm/(m ² .hr))
1	1018

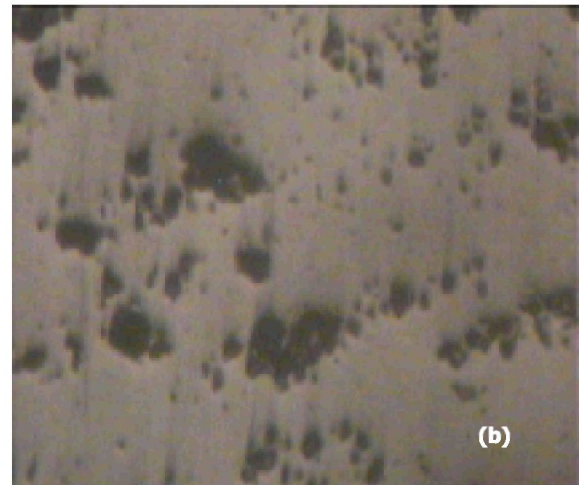
Table 7 : Corrosion rate of clad portion

Sl. No.	Heat input, Q (kJ/mm)	Corrosion rate (gm/(m ² .hr))
1	0.338	305
2	0.344	360
3	0.363	401
4	0.378	439
5	0.392	520
6	0.412	475

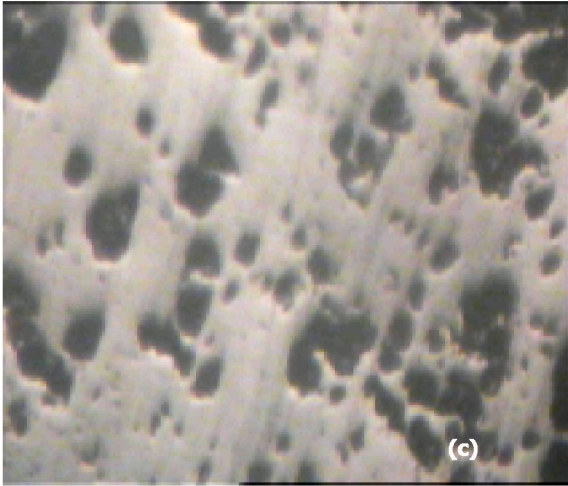
However, **Fig.4(d)** and **4(f)** indicate dense small corrosion pits with few big pits. Quite large pits that give correspondingly high corrosion rate are observed in **Fig.4(e)**.



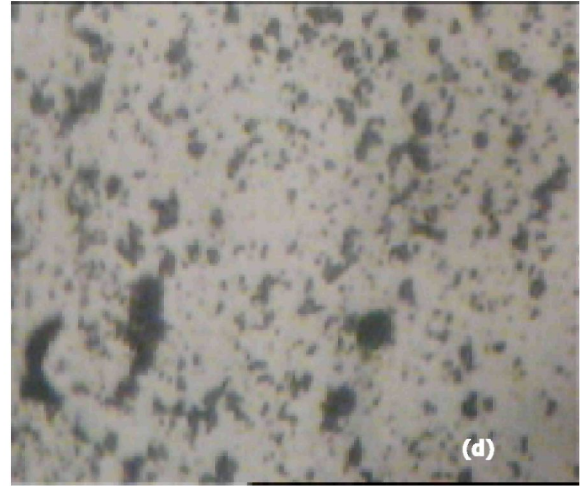
(a) V= 26 V, I= 145 A, S= 535.8 mm/min, Q= 0.338 kJ/mm, Sl. No.1,



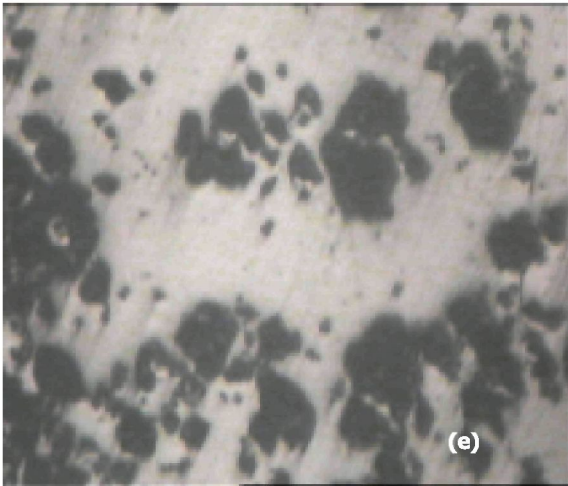
(b) V= 26 V, I= 130 A, S= 471.6 mm/min, Q= 0.344 kJ/mm, Sl. No.2,



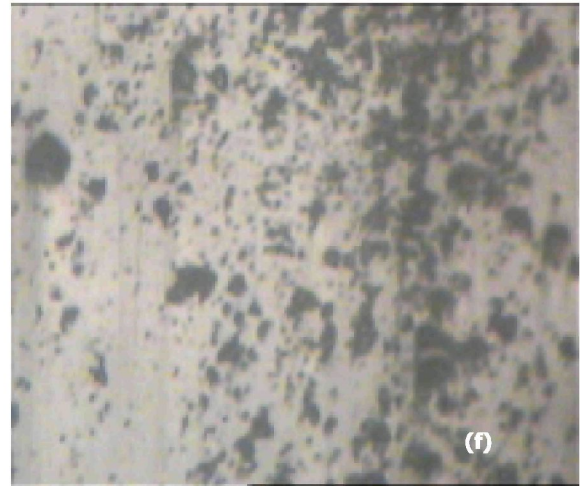
(c) V= 28 V, I= 145 A, S= 536.4 mm/min,
Q = 0.363 kJ/mm, Sl. No.3,



(d) V= 28 V, I= 145 A, S= 516 mm/min,
Q= 0.378 kJ/mm, Sl. No.4,



(e) V= 26 V, I= 130 A, S= 414 mm/min,
Q= 0.392 kJ/mm, Sl. No.5,



(f) V= 28 V, I= 145 A, S= 472.8 mm/min,
Q = 0.412 kJ/mm Sl. No.6

Fig. 4 : Micrographs (X200) of corrosion pits

Quite large corrosion rate of 1018 gm/m²hr is observed in bare unclad base plate as shown in **Table 6**. Presence of heat resistant and corrosion resistant alloying elements of the austenitic stainless steel electrode, that makes the weld bead, may have resulted in the low rate of corrosion.

4.0 CONCLUSIONS

From the present experimental investigation, the following may be concluded:

- There is a good amount of bonding between the base metal and weld deposition that is observed in the range of experiments done.
- Increase in heat input initially shows an increasing trend of penetration and reinforcement. After a level, decreasing nature of penetration and reinforcement is noted on the whole.
- Corrosion rate also increases with hike in heat input up to a level. Beyond this, further increase in heat input results in lowering of corrosion rate.
- Substantial improvement in corrosion resistance is observed in clad specimens under weld current of 145 A, weld voltage of 26 V and weld speed of 535.8 mm/min corresponding to 0.338 kJ/mm heat input within the range experiments performed, and hence, this condition may be adopted for weld cladding.

REFERENCES

- [1] Alam N, Jarvis L, Harris D and Solta A (2002); Laser cladding for repair of engineering components, *Australian Welding Journal*, 47, pp.38-47.
- [2] Ratkus A, Torims T and Gutakovskis V (2012); Research on bucket bore renewal technologies, *Proceedings of the 8th Int. DAAAM Baltic Conference*, Tallinn, Estonia, pp.1-5.
- [3] Kumar V, Singh G and Yusufzai MZK (2012); Effects of process parameters of gas metal arc welding on dilution in cladding of stainless steel on mild steel, *MIT International Journal of Mechanical Engineering*, 2(2), pp.127-131.
- [4] Murugan N and Parmar RS (1994); Effects of MIG process parameters on the geometry of the bead in the automatic surfacing of stainless steel, *Journal of Materials Processing Technology*, 41, pp.381s-398s.
- [5] Kannan T and Yoganandh J (2010); Effect of process parameters on clad bead geometry and its shape relationships of stainless steel claddings deposited by GMAW, *International Journal of Advanced Manufacturing Technology*, 47, pp.1083-1095.
- [6] Sabiruddin K, Das S and Bhattacharya S (2013); Selection of appropriate process parameters for gas metal arc welding of medium carbon steel specimens, *International Journal of Analytic Hierarchy Process*, 5(2); pp.252-267.
- [7] Sreeraj P, Kannan T and Maji S (2013); Prediction and control of weld bead geometry in gas metal arc welding process using simulated annealing algorithm, *International Journal of Computational Engineering Research*, 3(1), pp.213-222.
- [8] Sarkar A and Das S (2011); Application of grey-based taguchi method for optimizing gas metal arc welding of stainless steels, *Indian Welding Journal*, 44(1), pp.37-48.
- [9] Palani PK and Murugan N (2007); Optimisation of weld bead geometry for stainless steel cladding deposited by FCAW, *Journal of Materials Processing Technology*, 190, pp.291-299.
- [10] Ghosh PK, Gupta PC and Goyal VK (1998); Stainless steel cladding of structural steel plates using the pulsed current GMAW process, *Welding Research Supplement, Welding Journal*, pp.307s-314s.
- [11] Chakrabarti B, Das H, Das S and Pal TK (2013); Study on clad quality of duplex stainless steel by gas metal arc welding process, *Transactions of Indian Institute of Metals*, 66(3), pp.221-230.
- [12] Kannan T and Muguran N (2006); Effect of flux cored arc welding process parameters on duplex stainless steel clad quality, *Journal of Materials Processing Technology*, 176, pp.230-239.
- [13] Nouri M, Abdollah-Zadeh A and Malek F (2007); Effect of welding parameters on dilution and weld bead geometry in cladding, *Journal of Materials Science and Technology*, 23(6), pp.817-822.
- [14] Palani PK and Muguran N (2006); Development of mathematical models for prediction of weld bead geometry in cladding by flux cored arc welding, *International Journal of Advanced Manufacturing Technology*, 30, pp.669-676.
- [15] Khara B, Mandal ND, Sarkar A, Sarkar M, Chakarbarti B and Das S (2016); Weld cladding with austenitic stainless steel for imparting corrosion resistance, *Indian Welding Journal*, 49(1), pp.74-81.
- [16] Verma AK, Biswas BC, Roy P, De S, Saren S and Das S (2013); Exploring quality of austenitic stainless steel clad layer obtained by metal active gas welding, *Indian Science Cruiser*, 27(4), pp.24-29.
- [17] Rao NV, Reddy GM and Nagarjuna S (2011); Weld overlay cladding of high strength low alloy steel with austenitic stainless steel structure and properties, *Materials and Design*, 32, pp.2496-2506.
- [18] Tsai WT and Chen JR (2007); Galvanic corrosion between the constituent phases in duplex stainless steel, *Corrosion Science*, 49, pp.3659-3668.
- [19] Mondal A, Saha MK, Hazra R and Das S (2016); Influence of heat input on weld bead geometry using duplex stainless steel wire electrode on low alloy steel specimens, *Cogent Engineering*, 3(1), p.1143598.
- [20] Funderburk RS (1999); Key concepts in welding engineering, *Welding Innovation*, 16(1), pp.1-4.
- [21] Elmer JW, Allen SM and Eager TW (1989); Microstructural development during solidification of stainless steel alloys, *Metallurgical Transactions A*, 20A, pp.217-231.
- [22] Martins M and Casteletti LC (2005); Heat treatment temperature influence on ASTM A890 GR 6A super duplex stainless steel microstructure, *Materials Characterization*, 55(3), pp.225-233.